

Article

# Finite Element Study on the Wear Performance of Movable Jaw Plates of Jaw Crushers after a Symmetrical Laser Cladding Path

Yuhui Chen <sup>1,\*</sup>, Guoshuai Zhang <sup>1</sup>, Ruolin Zhang <sup>1</sup>, Timothy Gupta <sup>2,\*</sup> and Ahmed Katayama <sup>3</sup>

<sup>1</sup> School of Energy and Power Engineering, Zhengzhou University of Light Industry, Zhengzhou 450000, Henan, China; 331821010411@zzuli.edu.cn (G.Z.); 331921020487@zzuli.edu.cn (R.Z.)

<sup>2</sup> Queen Mary Research Institute of London, London E1 4NS, UK

<sup>3</sup> School of Electronic Engineering and Mechanical, New York University of Technology, New York, NY 10027, USA; nyutkatayama@nyut.us

\* Correspondence: chenyh@zzuli.edu.cn (Y.C.); mutimothy@qmril.gb (T.G.); Tel.: +1-006-662-8264 (T.G.)

Received: 19 April 2020; Accepted: 2 July 2020; Published: 7 July 2020



**Abstract:** At present, research on the influence of friction heat on the wear resistance of laser cladding layers is still lacking, and there is even less research on the temperature of laser cladding layers under different loads by a finite element program generator (FEPG). After a symmetrical laser cladding path, the wear performance of the moving jaw will change. The study of the temperature change of the moving jaw material in friction provides a theoretical basis for the surface modification of the moving jaw. The model of the column ring is built in a finite element program generator (FEPG). When the inner part of the column is WDB620 (material inside the cylinder) and the outer part is ceramic powder (moving jaw surface material), the relationship between the temperature and time of the contact surface is analyzed under the load between 100 and 600 N. At the same time, the stable temperature, wear amount, effective hardening layer thickness, strain thickness, and iron oxide content corresponding to different loads in a finite element program generator (FEPG) were analyzed. The results showed that when the load is 300 N, the temperature error between the finite element program generator (FEPG) and the movable jaw material is the largest, and the relative error is 4.3%. When the load increases, the stable temperature of the moving jaw plate increases after the symmetrical laser cladding path, and the wear amount first decreases and then increases. The minimum wear amount appears at a load of 400 N and a temperature of 340 °C; the strain thickness of the sample material increases gradually, and the effective hardening layer thickness increases. However, when the load reaches 400 N, the thickness of the effective hardening layer changes little; the content of Fe decreases gradually, and the content of FeO and Fe<sub>2</sub>O<sub>3</sub> increases. The increase of the moving jaw increases in turn the temperature of the laser cladding layer of the test jaw material, which intensifies the oxidation reaction of the ceramic powder of the laser cladding layer.

**Keywords:** jaw crusher; symmetrical laser cladding path; FEPG; wear

## 1. Introduction

The mobile jaw plate of a jaw crusher is under severe impact in humid and high temperature environments. In the world, there are approximately 200–300 thousand movable jaw plates damaged by wear every year, and the consumption of steel is approximately 60–72 thousand tons [1]. Each year, this directly causes a loss of more than one billion dollars [2]. Therefore, mining enterprises pay a huge price for it. In order to strengthen its wear resistance, the surface of the moveable jaw plate is usually treated by laser cladding and other methods [3]. Laser cladding technology is an advanced surface modification technology, which involves many disciplines, such as metal materials, metallurgy,

chemistry, and so on. It is found that the tensile strength and hardness of the coating are always higher than that of the substrate, and the performance is better than that of the substrate [4–7], no matter how the laser power is set in a certain range. However, the analysis of the effect of friction heat on the wear resistance of laser cladding materials remains to be discussed. Therefore, the analysis of the wear behavior and material structure of the moving jaw plate after the symmetrical laser cladding path under the action of reciprocating impact and friction has a positive significance for the study of the influence of temperature on the wear resistance of the moving jaw plate and the surface modification of the moving jaw plate.

For the study of wear of the jaw crusher and other mining crushers after laser cladding, the existing research methods are mainly theoretical calculation, test, and other methods [8–10]. Karan et al. analyzed the main wear area of the acceleration plate of the vertical impact crusher, changed the structural parameters and production parameters of the rotor, respectively, and explored the wear characteristics of the acceleration plate [11]. Drzymała et al. analyzed the mechanical characteristics and particle movement characteristics of the hammer head of the vertical shaft impact crusher through theoretical calculation and determined that impact wear is the main form of hammer head wear [12]. Limanskiy et al. analyzed the movement of the jaw plate of the jaw crusher through experiments and analyzed the wear on the jaw plate of the jaw crusher based on the microwear mechanism and failure of the jaw plate surface, so as to learn the reason for jaw plate wear when materials are broken [13]. Amanov et al. analyzed the change trends of the grain area, and hardness and wear of the chain wheel of the mine conveyor after treatment at different temperatures and times and finally obtained the best treatment temperature and time [14]. Baek et al. analyzed the kinematic characteristics of the materials in the cone crusher through theoretical calculation, solved the crushing process, and obtained the compression ratio, particle size distribution coefficient, and crushing pressure in each region of the crushing chamber [15]. Abuhasel et al. calculated and analyzed the wear of the impact crusher plate hammer after different laser cladding processes and determined the spot diameter and powder spreading speed of laser cladding in the early stage with the minimum wear amount [16]. Anticoi et al. conducted an experimental analysis on the temperature field of the friction stir welding process on the roller surface of the roller crusher and found that the friction coefficient decreased with the increase of the temperature, and the welding temperature increased with the increase of the concave angle of the shoulder [17]. Pei et al. analyzed the influence of particle size on the liner wear of the semi-autogenous mill via a theoretical calculation method. The results showed that the wear of the lining plate is especially significant when the particle size increases, the wear of the lining plate increases with the increase of particle size, and the kinetic energy obtained by large particle materials is far greater than that of small particle materials [18].

The wear amount calculated by theory is quite different from the actual result, and most of the conditions calculated by theory are ideal. In the physical prototype, the wear performance test of the components of the crusher is carried out, and the analysis of the wear characteristics of the components has great data disturbance, so it is difficult to extract the relevant data accurately and collect the data. Therefore, in this study, a finite element model of the cylinder-ring was built in the finite element program generator (FEPG). The temperature of laser cladding ceramic powder (surface material of the movable jaw plate) obtained by FEPG under different loads was verified and compared with the temperature obtained by the test. At the same time, the stable temperature, wear amount, effective hardening layer thickness, strain thickness, and iron oxide content corresponding to different loads were analyzed. The research results can be used to solve the problems of failure of the jaw crusher caused by high friction temperature and low service life of the moving jaw plate under complex working conditions. At the same time, they can provide a theoretical basis for analyzing the wear performance of the moving jaw plate material after symmetrical laser cladding path and the temperature change of the moving jaw plate in friction, which is of great significance to the surface modification of the moving jaw plate.

In addition, through the existing literature, it is found that in the cylinder disk test, along the direction of sliding friction, plastic deformation occurs on the surface of cylinder coating, resulting in different thicknesses of the work hardening layer [19–21]. However, analysis of the effect of friction heat on the wear resistance of laser cladding materials is still lacking.

## 2. Materials and Methods

In this study, WDB620 (Figure 1) was selected as the material of the moving jaw plate, and then the ceramic powder was laser-cladded on the surface of the moving jaw plate. The contents of various chemical components of ceramic powder are shown in Table 1 [22–25].



Figure 1. WDB620 material.

Table 1. Chemical composition.

Mn (%)	Rb (%)	C (%)	P (%)	V (%)	B (%)	Re (%)	Fe (%)
2.2	1.3	22.5	0.3	1.2	1.7	3.8	26.4

The cylinder sample after cutting is installed on the friction electronic tester and closely contacts with the ring. The material of the ring is 40Cr, the loads of the cylinder sample are 100, 200, 300, 400, 500, and 600 N, and the rotation speed of the ring is 2000 r/min. The test scheme was carried out according to Table 2.

Table 2. Test plan.

Serial Number	Load $X_1/N$	Time $X_2/s$	Speed $X_3/s$
1	100	550	2000
2	200	550	2000
3	300	550	2000
4	400	550	2000
5	500	550	2000
6	600	550	2000

Through the thermocouple temperature sensor used to collect the temperature of the cylinder sample (Figure 2), the collected temperature of each point is counted.

The model of the cylinder-ring was built in UG (Figure 3). (UG is an interactive computer-aided design and computer-aided manufacturing software, which has powerful functions and can realize the construction of various complex entities and models. It is mainly used in the product development fields of mechanical product modeling design, structural design, part assembly design, mold design, numerical control programming, design analysis, etc.) The radius difference between the two concentric circles is 230 mm [26–30], and it is added to the creator in FEPC in the form of  $x_t$  (Figure 4). The material of the setting ring in FEPC is 40Cr, the inner part of the cylinder is WDB620 (movable jaw plate

material), and the outer part is laser cladding ceramic powder. The specific physical parameter settings of the cylinder-ring are shown in Table 3 [31–34].

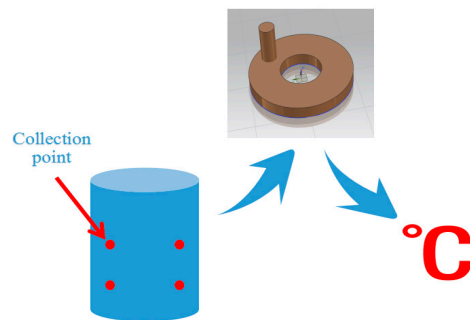


Figure 2. Thermocouple temperature sensor.

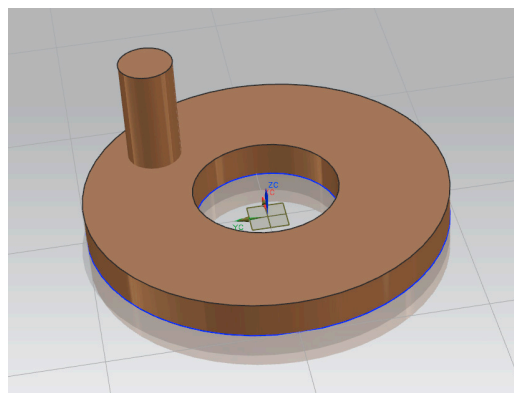


Figure 3. Cylinder-ring model in UG.

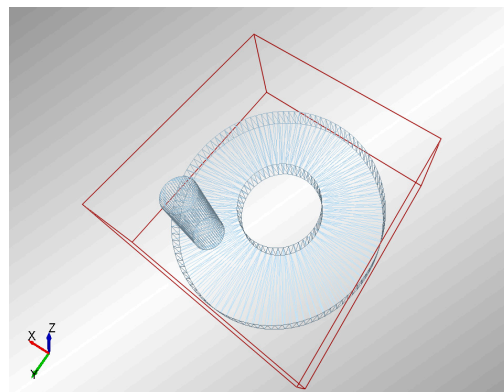


Figure 4. Cylinder-ring model in a finite element program generator (FEPG).

Table 3. Parameter setting in FEPG.

Material	40Cr	WDB620	Ceramic Powder
Shear modulus (Pa)	$2.06 \times 10^{12}$	$2.26 \times 10^{11}$	$4.16 \times 10^{11}$
Heat transfer coefficient ( $W/(m \cdot k)$ )	35	60	72
Density ( $kg/m^3$ )	7220	8230	7850

### 3. Results and Discussion

#### 3.1. FEPG and Test Results

The finite element study [35–37] was carried out under the loads of 100, 200, 300, 400, 500, and 600 N, respectively, and the rotating speed of the ring was 2000 r/min. The maximum surface temperature and radial diffusion size of the ring under different loads were obtained (Figure 5).

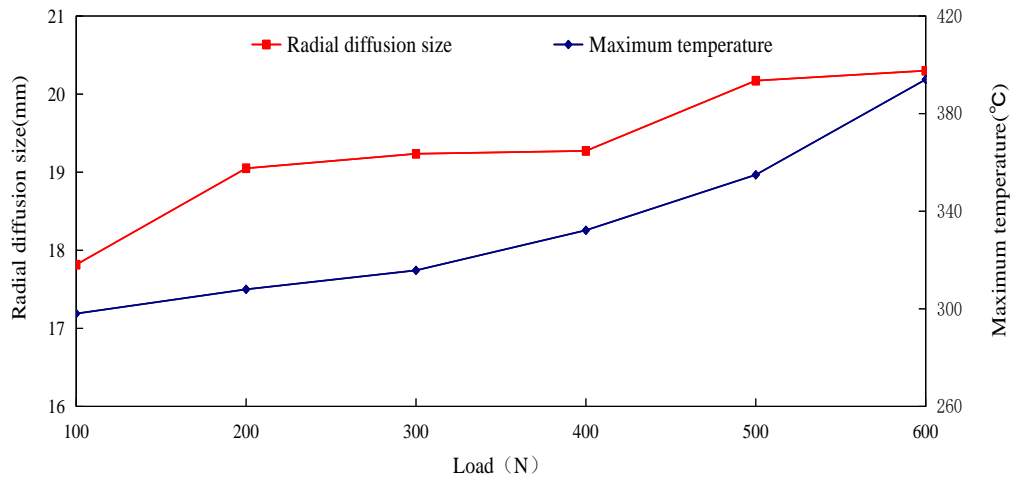


**Figure 5.** Maximum value and radial diffusion size of ring surface temperature.

The maximum temperature and radial diffusion size in Figure 5 are analyzed. When the cylinder loads are 100, 200, 300, 400, 500, and 600 N, the maximum corresponding temperature is 396.8 °C and the radial diffusion size is 20.3 mm. With the increase of the load on the cylinder, the maximum temperature and the radial diffusion size of the ring surface are increasing.

When the cylinder loads are 100, 200, 300, 400, 500, and 600 N, the temperature change rule of the cylinder-ring contact surface is studied (Figure 6).

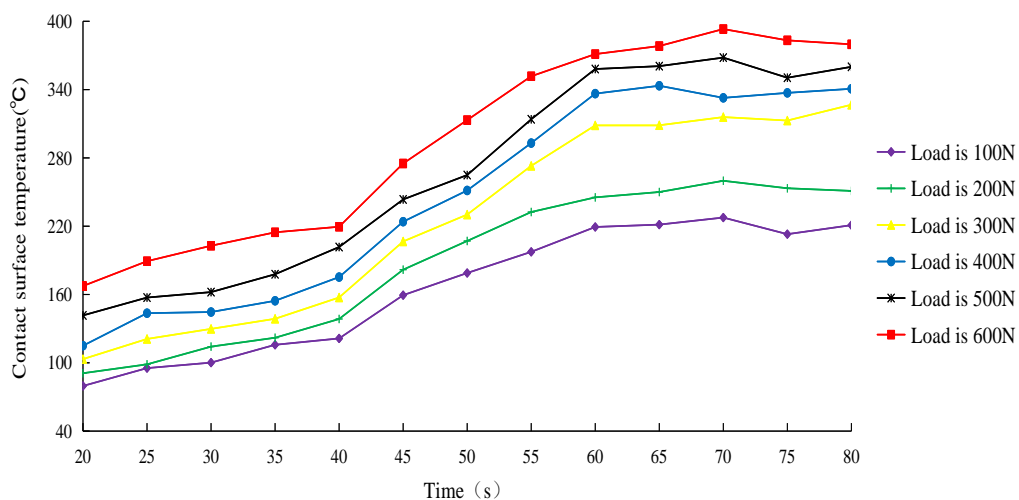


**Figure 6.** Temperature of cylinder-ring contact surface.

The temperature of the contact surface in Figure 6 is analyzed. At the same time, the temperature of the contact surface of the cylinder increases with the increase of the load on the cylinder. However, the change trend of contact surface temperature under different loads is basically the same. After the time reaches about 60 s, the temperature does not rise significantly. When the cylinder loads are 100,

200, 300, 400, 500, and 600 N, the contact surface temperature is stable at 222, 251, 326, 341, 360, and 378 °C, respectively.

Through the test, the mean value of the temperature at the acquisition point under the sample loads of 100, 200, 300, 400, 500, and 600 N is obtained. The test result data are processed by high-order function regression through SPSS software (12.0, SPSS Inc., Chicago, IL, USA), and the regression function of temperature relative to time and load is as follows:

$$L = 600.421 - 3.252X_1 - 8.002X_2 + 1.763X_1X_2 - 0.287X_1^2 - 0.891X_2^2 \quad (1)$$

The temperature of the contact surface under different time and load is shown in Figure 7.

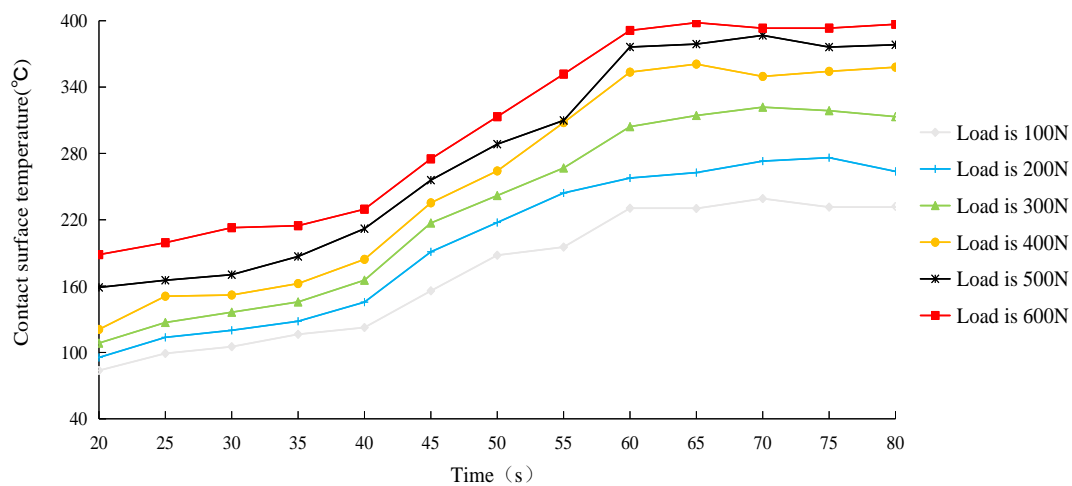


Figure 7. Temperature obtained at different times.

From Figure 7, when the load of the sample increases from 100 to 600 N, the temperature corresponding to the fixed time increases. When the loads of the sample are 100, 200, 300, 400, 500, and 600 N, the temperature of test and FEFG changes with time (Figure 8).

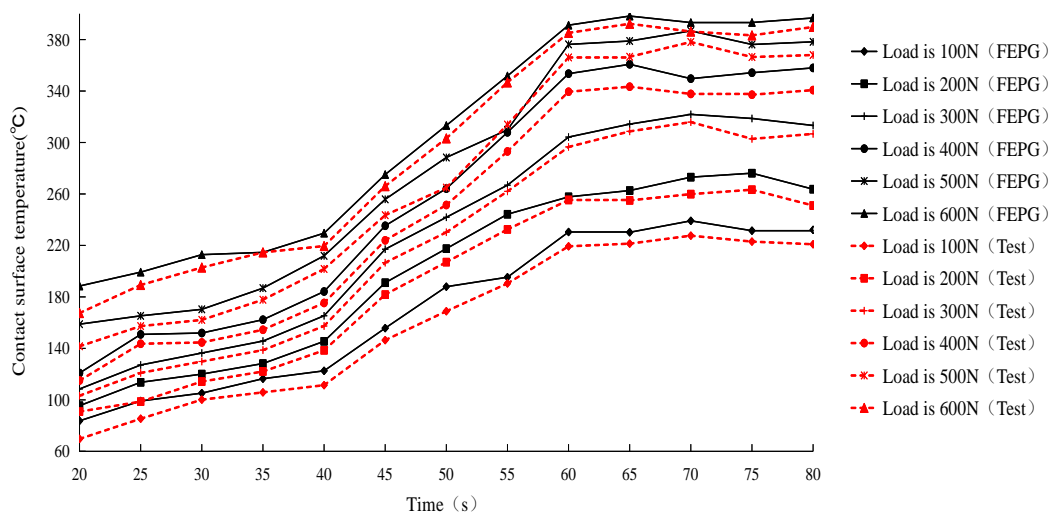


Figure 8. Comparison between test and FEFG.

From Figure 8, when the sample loads are 100, 200, 300, 400, 500, and 600 N, the temperature obtained by FEFG at the same time point is slightly higher than the test result. The reason for the result is that there are many environmental effects, such as heat and air transfer loss, in the actual test.

However, when the loads of FEFG are 100, 200, 300, 400, 500, and 600 N, the trend of temperature change is the same, and when the load is 400 N and the time is 80 s, the temperature error is the largest, and the relative error is only 4.3%.

### 3.2. Effect of Temperature on the Performance of the Moving Jaw

According to the previous test and FEFG study, after a certain period of time (this study is about 65 s), the temperature of the moving jaw material sample tends to be stable, so the performance of the stabilized moving jaw material is analyzed. The steady temperature and wear of the cylinder under different loads are analyzed (Figure 9).

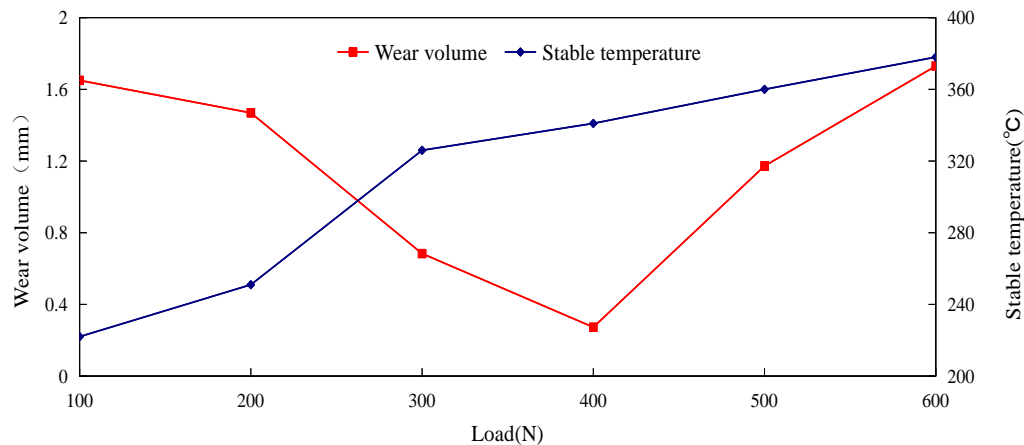


Figure 9. Change trend of temperature and wear.

With the increase of load, the stable temperature rises gradually, and the wear amount rises after an initial decrease. When the load is at 400 N and the temperature is around 340 °C, the value is the smallest. This is because the laser cladding layer on the surface of the sample material (moving jaw material) is partially melted under high heat, which reduces the wear. However, the temperature and load continue to increase, which not only destroys the protective layer, but also causes part of the remaining protective layer to bond and tear due to the rotation of the ring.

Through the electron microscope, the effective hardening layer thickness and strain thickness of the moving jaw specimen under different loads were analyzed, and the results were compared (Figure 10).

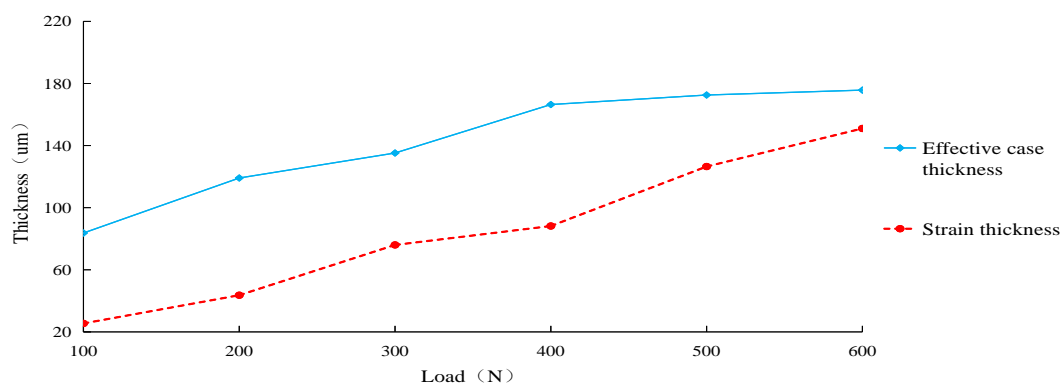


Figure 10. Effective hardening layer thickness and strain thickness

Through the analysis of the effective hardening layer thickness and strain thickness under no load, it is known that with the increase of load, the strain thickness of the sample material increases gradually, and the effective hardening layer thickness increases significantly, but when the load reaches

400 N, the effective hardening layer thickness changes little. The results show that when the load is about 400 N, the wear resistance of the laser cladding material is relatively good.

The surface of the sample was analyzed by X-ray photoelectron spectroscopy (XPS), and the content changes of Fe, O, Mn, C, V, and Re were counted (Figure 11).

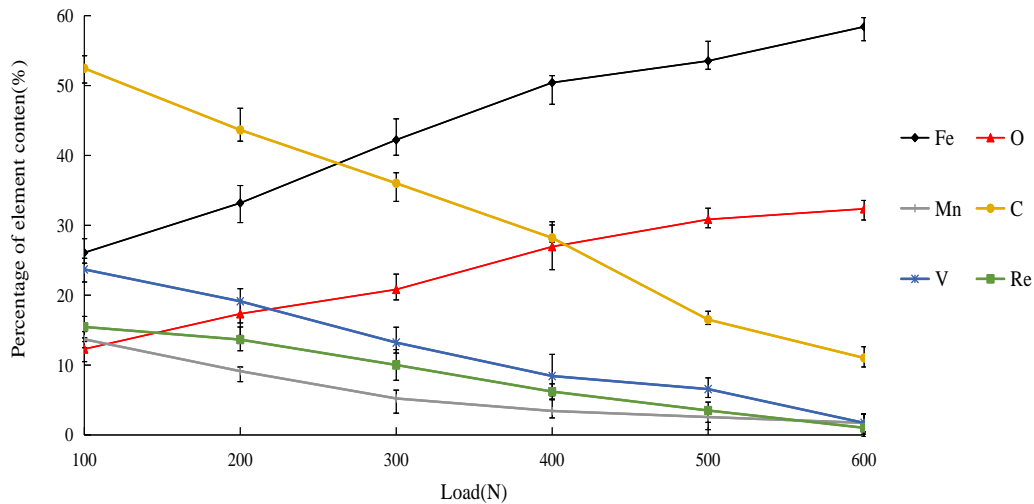


Figure 11. Content change of Fe, O, Ti, Cr, V, and Nb.

It can be seen from Figure 11 that there are mainly Fe, O, Mn, V, and other elements on the surface of the wear mark of the material, and the mass fraction of Fe and O elements accounts for the largest proportion. With the increase of the load, the mass fraction of Fe element increases from 26.08% to 58.42%, and the mass fraction of O element increases from 12.28% to 32.37%. With the increase of the load on the sample, the content of Fe and O increases gradually. In the process of friction, the increase of the load on the cylinder causes the temperature of the friction contact surface of the cylinder to rise, and the constant formation of iron oxide, which leads to the oxidation and wear of the deposition layer of the cylinder.

Analyzing the content of different types of iron oxide in the laser cladding layer of the moving jaw plate, A represents Fe, B represents FeO, and C represents Fe<sub>2</sub>O<sub>3</sub> (Figure 12).

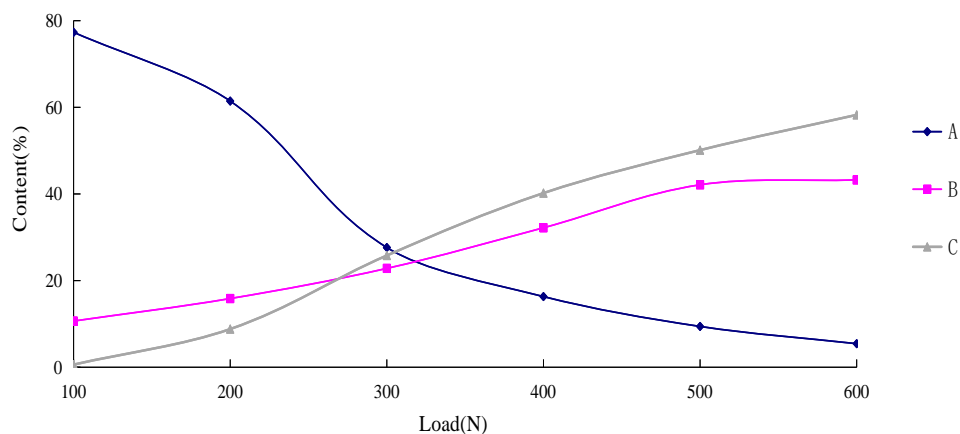


Figure 12. Content of Fe, FeO, and Fe<sub>2</sub>O<sub>3</sub>.

The contents of Fe, FeO, and Fe<sub>2</sub>O<sub>3</sub> were studied. It was found that when the load was 100 N, the oxide on the worn surface was mainly Fe, and then there is not only FeO, but also Fe<sub>2</sub>O<sub>3</sub> when the load is 200 and 300 N. With the increase of load from 400 to 600 N, the content of FeO and Fe<sub>2</sub>O<sub>3</sub> on the worn surface of the coating continued to increase. In the above analysis, it can be found that

with the increase of friction temperature, the high-temperature transformation process of wear on the surface is  $\text{Fe} \rightarrow \text{FeO} \rightarrow \text{Fe}_2\text{O}_3$ . The main reason is that in the process of friction and wear, the micro convex particles on the contact surface easily produce a flash point temperature (higher than  $1500^\circ$ ) under the conditions of high load and high speed, and the changes of temperature and load affect the change of oxide type [38–40]. The simulation experiment is in an ideal working environment where there are no micro convex particles on the surface of the friction pair and there is no flash point high temperature. In the experiment of temperature measurement, the temperature changes dynamically, and the temperature of the contact surface is the highest. The thermocouple only measures the surface temperature, so it cannot measure the flash point temperature. Thus, the main reason for the existence of the iron oxide is that the heat generated by friction is accumulating in the contact surface, which leads to the plastic deformation of the material surface caused by oxidation and softening, and the appearance of the friction oxide layer. The results show that the increase of the sample load increases the temperature of the laser cladding layer of the sample material (movable jaw plate material), which intensifies the oxidation reaction of the ceramic powder of the laser cladding layer.

#### 4. Conclusions

Based on the theory of tribology and heat transfer, focusing on the influence of temperature on the properties of laser cladding ceramic powder (surface material of the movable jaw plate), the coupling analysis of cylinder disc wear is completed using the finite element software FEPA, and a temperature measurement test bench which is built on the wear test machine for test analysis and verification. Finally, the wear amount, effective hardening layer thickness, and strain thickness of the moving jaw after symmetrical laser cladding path are analyzed by FEPA. It is concluded that in the wear process of the moving jaw material after the symmetrical laser cladding path, the maximum temperature of the moving jaw material is related to its load.

It is found that when the load is 100, 200, 300, 400, 500, and 600 N and the time is about 65 s, the contact surface temperature is stable at 222, 251, 326, 341, 360, and  $378^\circ\text{C}$ , respectively. The results show that the temperature of FEPA at the same time point is slightly higher than that of the test when the loads of the sample are 100, 200, 300, 400, 500, and 600 N, but the trend of temperature change is the same. When the load is 300 N, the temperature error between the test and FEPA is the largest, and the relative error is only 4.3%. When the load increases, the stable temperature of the laser-cladded moving jaw material increases, and the wear amount first decreases and then increases. The minimum wear amount appears at the load of 400 N, and the temperature is about  $320^\circ\text{C}$ . With the increase of load, the thickness of strain increases gradually, and the thickness of the effective hardening layer increases obviously, but when the load reaches 400 N, the thickness of the effective hardening layer changes little. The increase of the sample load increases in turn the temperature of the laser cladding layer of the sample material, which intensifies the oxidation reaction of the ceramic powder of the laser cladding layer. The research results provide a new idea for the analysis of the wear behavior of the moving jaw plate after laser cladding under the action of reciprocating impact and friction and provide a theoretical basis for the analysis of the change of the wear resistance of the moving jaw plate caused by the temperature and the surface modification of the moving jaw plate.

**Author Contributions:** Conceptualization, Y.C. and T.G.; data curation, Y.C., G.Z., R.Z., T.G. and A.K.; formal analysis, Y.C., G.Z., R.Z., T.G. and A.K.; funding acquisition, Y.C.; investigation, Y.C.; resources, Y.C.; software, Y.C., G.Z., R.Z. and T.G.; supervision, Y.C. and T.G.; visualization, Y.C. and G.Z.; writing—original draft preparation, Y.C., G.Z., R.Z., T.G. and A.K.; writing—review and editing, Y.C., G.Z., R.Z. and T.G. All authors have read and agreed to the published version of the manuscript.

**Funding:** This work is supported by the National Natural Science Foundation of China Youth Foundation (no.51705474).

**Acknowledgments:** The authors thank the anonymous editor for the editing assistance. Lastly, the authors would like to thank the anonymous reviewers for their valuable comments and suggestions on an earlier version of our manuscript.

**Conflicts of Interest:** The authors declare that they have no conflict of interest.

## References

1. Jiang, J.; Xie, Y.; Qian, W.; Hall, R. Important factors affecting the gouging abrasion resistance of materials. *Miner. Eng.* **2018**, *128*, 238–246. [[CrossRef](#)]
2. Deepak, B.B.; Bahubalendruni, M.V. Numerical analysis for force distribution along the swing jaw plate of a single toggle jaw crusher. *World J. Eng.* **2017**, *14*, 255–260. [[CrossRef](#)]
3. Liu, R.; Shi, B.; Li, G.; Yu, H. Influence of operating conditions and crushing chamber on energy consumption of cone crusher. *Energies* **2018**, *11*, 1102. [[CrossRef](#)]
4. Li, Y.; Zhang, P.; Bai, P.; Su, K.; Su, H. TiBCN-Ceramic-Reinforced Ti-Based Coating by Laser Cladding: Analysis of Processing Conditions and Coating Properties. *Coatings* **2019**, *9*, 407. [[CrossRef](#)]
5. Gabriel, T.; Rommel, D.; Scherm, F.; Gorywoda, M.; Glatzel, U. Symmetrical laser cladding path of ultra-thin nickel-based superalloy sheets. *Materials* **2017**, *10*, 279. [[CrossRef](#)]
6. Yan, X.-L.; Dong, S.-Y.; Xu, B.-S.; Cao, Y. Progress and challenges of ultrasonic testing for stress in remanufacturing symmetrical laser cladding path coating. *Materials* **2018**, *11*, 293. [[CrossRef](#)]
7. Xu, Z.; Wang, Z.; Chen, J.; Qiao, Y.; Zhang, J.; Huang, Y. Effect of rare earth oxides on microstructure and corrosion behavior of laser-cladding coating on 316L stainless steel. *Coatings* **2019**, *9*, 636. [[CrossRef](#)]
8. Pang, X.; Wei, Q.; Zhou, J.; Ma, H. High-temperature tolerance in multi-scale cermet solar-selective absorbing coatings prepared by symmetrical laser cladding path. *Materials* **2018**, *11*, 1037. [[CrossRef](#)]
9. Lian, G.; Zhang, H.; Zhang, Y.; Tanaka, M.L.; Chen, C.; Jiang, J. Optimizing processing parameters for multi-track symmetrical laser cladding path utilizing multi-response grey relational analysis. *Coatings* **2019**, *9*, 356. [[CrossRef](#)]
10. Wang, S.; Liu, C. Real-time monitoring of chemical composition in nickel-based symmetrical laser cladding path layer by emission spectroscopy analysis. *Materials* **2019**, *12*, 2637. [[CrossRef](#)]
11. Karan, S.K.; Samadder, S.R. Reduction of spatial distribution of risk factors for transportation of contaminants released by coal mining activities. *J. Environ. Manag.* **2016**, *180*, 280–290. [[CrossRef](#)] [[PubMed](#)]
12. Drzymała, T.; Zegardło, B.; Tofilo, P. Properties of concrete containing recycled glass aggregates produced of exploded lighting materials. *Materials* **2020**, *13*, 226. [[CrossRef](#)] [[PubMed](#)]
13. Limanskiy, A.V.; Vasilyeva, M.A. Using of low-grade heat mine water as a renewable source of energy in coal-mining regions. *Ecol. Eng.* **2016**, *91*, 41–43. [[CrossRef](#)]
14. Amanov, A.; Ahn, B.; Lee, M.G.; Jeon, Y.; Pyun, Y. Friction and wear reduction of eccentric journal bearing made of sn-based babbitt for ore cone crusher. *Materials* **2016**, *9*, 950. [[CrossRef](#)]
15. Baek, J.; Choi, Y. Deep neural network for ore production and crusher utilization prediction of truck haulage system in underground mine. *Appl. Sci.* **2019**, *9*, 4180. [[CrossRef](#)]
16. Abuhasel, K.A. A comparative study of regression model and the adaptive neuro-fuzzy conjecture systems for predicting energy consumption for jaw crusher. *Appl. Sci.* **2019**, *9*, 3916. [[CrossRef](#)]
17. Anticoi, H.; Guasch, E.; Ahmad Hamid, S.; Oliva, J.; Alfonso, P.; Bascompta, M.; Sanmiquel, L.; Escobet, T.; Escobet, A.; Parcerisa, D.; et al. An improved high-pressure roll crusher model for tungsten and tantalum ores. *Minerals* **2018**, *8*, 483. [[CrossRef](#)]
18. Pei, Z.; Galindo-Torres, S.A.; Tang, H.; Jin, G.; Scheuermann, A.; Ling, L. An efficient discrete element lattice boltzmann model for simulation of particle-fluid, particle-particle interactions. *Comput. Fluids* **2017**, *147*, 63–71.
19. Ren, X.; Liu, Z. Influence of cutting parameters on work hardening behavior of surface layer during turning superalloy Inconel 718. *Int. J. Adv. Manuf. Technol.* **2016**, *86*, 2319–2327. [[CrossRef](#)]
20. Gao, P.; Wei, K.; Hanchen, Y.U.; Yang, J.; Wang, Z.; Zeng, X. Influence of layer thickness on microstructure and mechanical properties of selective laser melted Ti-5Al-2.5Sn alloy. *Acta Metall. Sin.* **2018**, *54*, 999–1009.
21. Nishida, Y.; Yokoyama, S. Mechanisms of temperature dependence of threshold voltage in high-k/metal gate transistors with different TiN thicknesses. *Int. J. Electron.* **2016**, *103*, 629–647. [[CrossRef](#)]
22. Cuomo, S.; Chareyre, B.; D'Arista, P.; Sala, M.D.; Cascini, L. Micromechanical modelling of rainsplash erosion in unsaturated soils by finite element method. *Catena* **2016**, *147*, 146–152. [[CrossRef](#)]
23. Kroupa, M.; Vonka, M.; Soos, M.; Kosek, J. Utilizing the finite element method for the modeling of viscosity in concentrated suspensions. *Langmuir* **2016**, *32*, 8451–8460. [[CrossRef](#)] [[PubMed](#)]

24. Fallahnezhad, K.; Oskouei, R.H.; Badnava, H.; Taylor, M. An adaptive finite element simulation of fretting wear damage at the head-neck taper junction of total hip replacement: The role of taper angle mismatch. *J. Mech. Behav. Biomed. Mater.* **2017**, *75*, 58–67. [[CrossRef](#)]
25. Shinde, T.; Dhokey, N.B. Influence of carbide density on surface roughness and quasi-stable wear behaviour of h13 die steel. *Surf. Eng.* **2017**, *33*, 1–9. [[CrossRef](#)]
26. Soltani, R.; Sohi, M.H.; Ansari, M.; Haghighi, A.; Ghasemi, H.M.; Haftlang, F. Evaluation of niobium carbide coatings produced on aisi l2 steel via thermo-reactive diffusion technique. *Vacuum* **2017**, *146*, 44–51. [[CrossRef](#)]
27. Liu, G.; Sun, W.C.; Lowinger, S.M.; Zhang, Z.H.; Ming, H.; Peng, J. Coupled flow network and finite element modeling of injection-induced crack propagation and coalescence in brittle rock. *Acta Geotech.* **2018**, *14*, 1–26.
28. Thomas, J.J.; Ii, J.J.V.; Craddock, P.R.; Bake, K.D.; Pomerantz, A.E. The neutron scattering length density of kerogen and coal as determined by ch 3 oh/cd 3 oh exchange. *Fuel* **2014**, *117*, 801–808. [[CrossRef](#)]
29. Indimath, S.; Shunmugasundaram, R.; Balamurugan, S.; Das, B.; Singh, R.; Dutta, M. Ultrasonic technique for online measurement of bulk density of stamp charge coal cakes in coke plants. *Fuel Process. Technol.* **2018**, *172*, 155–161. [[CrossRef](#)]
30. Wang, Q.; Zeng, X.; Chen, C.; Lian, G.; Huang, X. An integrated method for multi-objective optimization of multi-pass Fe50/TiC symmetrical laser cladding path on AISI 1045 steel based on grey relational analysis and principal component analysis. *Coatings* **2020**, *10*, 151. [[CrossRef](#)]
31. Yu, J.; Sun, W.; Huang, H.; Wang, W.; Wang, Y.; Hu, Y. Crack sensitivity control of nickel-based laser coating based on genetic algorithm and neural network. *Coatings* **2019**, *9*, 728. [[CrossRef](#)]
32. Wu, F.; Chen, T.; Wang, H.; Liu, D. Effect of Mo on microstructures and wear properties of in situ synthesized Ti(C,N)/Ni-based composite coatings by symmetrical laser cladding path. *Materials* **2017**, *10*, 1047. [[CrossRef](#)] [[PubMed](#)]
33. Li, C.; Liu, C.; Li, S.; Zhang, Z.; Zeng, M.; Wang, F.; Wang, J.; Guo, Y. Numerical simulation of thermal evolution and solidification behavior of symmetrical laser cladding path AISiTiNi composite coatings. *Coatings* **2019**, *9*, 391. [[CrossRef](#)]
34. Li, Y.; Chen, T.; Liu, D. Path planning for symmetrical laser cladding path robot on artificial joint surface based on topology reconstruction. *Algorithms* **2020**, *13*, 93. [[CrossRef](#)]
35. Wang, Y.; Liang, Z.; Zhang, J.; Ning, Z.; Jin, H. Microstructure and antiwear property of symmetrical laser cladding path Ni–Co duplex coating on copper. *Materials* **2016**, *9*, 634. [[CrossRef](#)]
36. Yang, K.; Xie, H.; Sun, C.; Zhao, X.; Li, F. Influence of vanadium on the microstructure of IN718 alloy by symmetrical laser cladding path. *Materials* **2019**, *12*, 3839. [[CrossRef](#)]
37. Chen, J.; Zhou, Y.; Shi, C.; Mao, D. Microscopic analysis and electrochemical behavior of Fe-based coating produced by symmetrical laser cladding path. *Metals* **2017**, *7*, 435. [[CrossRef](#)]
38. Lu, H.; Zhang, P.; Ren, S.; Guo, J.; Li, X.; Dong, G.I. The preparation of polytrifluorochloroethylene (PCTFE) micro-particles and application on treating bearing steel surfaces to improve the lubrication effect for copper-graphite (Cu/C). *Appl. Surf. Sci.* **2018**, *427*, 1242–1247. [[CrossRef](#)]
39. Zori, M.H.; Soleimanigorgani, A. Ink-jet printing of micro-emulsion TiO<sub>2</sub> nano-particles ink on the surface of glass. *Journal Eur. Ceram. Soc.* **2012**, *32*, 4271–4277. [[CrossRef](#)]
40. Feigenbaum, E.; Raman, R.N.; Cross, D.A.; Carr, C.W.; Matthews, M.J. Laser-induced Hertzian fractures in silica initiated by metal micro-particles on the exit surface. *Opt. Express* **2016**, *24*, 10527–10536. [[CrossRef](#)]

